Quantification of Resolution in Multiplanar Reconstructions for Digital Breast Tomosynthesis

Trevor L. Vent, Raymond J. Acciavatti, Young Joon Kwon, Andrew D. A. Maidment
University of Pennsylvania Health System, Department of Radiology, 3400 Spruce Street, Philadelphia, PA 19104 USA

ABSTRACT

Multiplanar reconstruction (MPR) in digital breast tomosynthesis (DBT) allows tomographic images to be portrayed in various orientations. We have conducted research to determine the resolution of tomosynthesis MPR. We built a phantom that houses a star test pattern to measure resolution. This phantom provides three rotational degrees of freedom. The design consists of two hemispheres with longitudinal and latitudinal grooves that reference angular increments. When joined together, the hemispheres form a dome that sits inside a cylindrical encasement. The cylindrical encasement contains reference notches to match the longitudinal and latitudinal grooves that guide the phantom's rotations. With this design, any orientation of the star-pattern can be analyzed. Images of the star-pattern were acquired using a DBT mammography system at the Hospital of the University of Pennsylvania. Images taken were reconstructed and analyzed by two different methods. First, the maximum visible frequency (in line pairs per millimeter) of the star test pattern was measured. Then, the contrast was calculated at a fixed spatial frequency. These analyses confirm that resolution decreases with tilt relative to the breast support. They also confirm that resolution in tomosynthesis MPR is dependent on object orientation. Current results verify that the existence of super-resolution depends on the orientation of the frequency; the direction parallel to x-ray tube motion shows super-resolution. In conclusion, this study demonstrates that the direction of the spatial frequency relative to the motion of the x-ray tube is a determinant of resolution in MPR for DBT.

Keywords: Digital breast tomosynthesis (DBT), multiplanar reconstruction, super-resolution, phantom, anisotropy, contrast.

1. INTRODUCTION

Multiplanar reconstruction (MPR) in computed tomography (CT) is considered valid and serves as the gold standard for MPR in any form of x-ray tomography. This is expected of CT because CT images are reconstructed from a sufficient set of projections (e.g., 0° to 180° + fan angle, or 0° to 360°). Traditionally, CT scanners produce axial images, although it is possible to produce reconstructions having different orientations. Often, this allows disease to be better portrayed[1].

Digital breast tomosynthesis (DBT) is still relatively new as a diagnostic imaging modality. The full capabilities of DBT are still unknown. Like CT scans, the best method of reconstruction for each scan might not be the conventional reconstruction in slices parallel to the breast support. Viewing DBT images in an oblique plane can be advantageous, as we demonstrated in 2013[2].

High-contrast resolution patterns are commonly used to test the capabilities and limitations of x-ray imaging. Two applicable measures for resolution patterns are the limiting spatial resolution and modulation contrast. In this study, we used a star resolution pattern to test resolution and contrast of MPR for a commercial DBT system. By optimizing MPR for DBT, breast-imaging diagnostics can be improved and radiologists will have more tools at their disposal for DBT.

The purpose of this study is to demonstrate that DBT is capable of oblique multiplanar reconstructions and to quantify the quality of those reconstructions. This is done by analyzing limiting spatial resolution and contrast at various oblique orientations. We have designed and built a phantom to achieve these specific goals. This research is supplemental to research conducted with multiplanar reconstructions in 2013[2,3]. That study was limited to one rotation, while this research addresses more planar orientations. The reconstructions are oriented to view the star pattern in the plane for which it is rotated instead of viewing planes parallel to the breast support as most conventional software does. This project was conducted to guide the design of new tomosynthesis imaging systems.

Medical Imaging 2016: Physics of Medical Imaging, edited by Despina Kontos, Thomas G. Flohr, Joseph Y. Lo,
Proc. of SPIE Vol. 9783, 978303 · © 2016 SPIE · CCC code: 1605-7422/16/$18 · doi: 10.1117/12.2216260

2. METHODS

2.1 Phantom design & fabrication

To vary the star-pattern orientation with three degrees of freedom, a multiplanar reconstruction phantom (referred to as the dome phantom) was designed with SolidWorks (Dassault Systèmes, Vélizy-Villacoublay, France). The phantom is a dome with two separate hemispheres. Each hemisphere has longitudinal and latitudinal lines on the surface. They are incremented from the center of the dome in 15° increments according to two perpendicular axes – just like a globe. Inside, it has a cylindrical cavity that houses the star pattern. The dome is placed in a cylindrical encasement with a hemispherical cavity that contains 15° notches. The notches correspond to the grooves on the surface of the dome and guide the dome in its rotations. The point where the longitudinal lines converge is referred to as the apex. This axis of rotation goes through both apices. A test object is inserted into the middle of the dome phantom, inside of a shallow cylindrical cavity. An illustration of the design of the dome phantom can be seen in Figure 1.

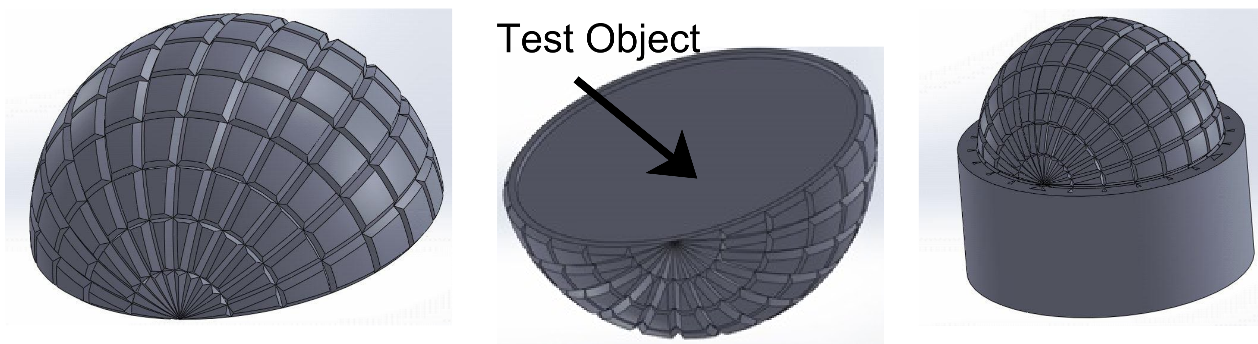

(a) (b) (c)

Figure 1: Dome Phantom design. It consists of the (a) top hemisphere with star apex, (b) bottom hemisphere with apex and cylindrical cavity (shallow) that houses the test object, and (c) dome phantom in cylindrical encasement with the apex at the 0° dome rotation (top half of the cylindrical encasement is removed for clarity).

Following its design, the phantom was printed using a 3D printer (Stratasys UPrint SE Plus, Rehovot, Israel). The material used was ABSPlus filament, which has a low x-ray attenuation coefficient, to minimize interference with the star pattern images and resultantly the modulation contrast. Figure 2 shows the finished product.

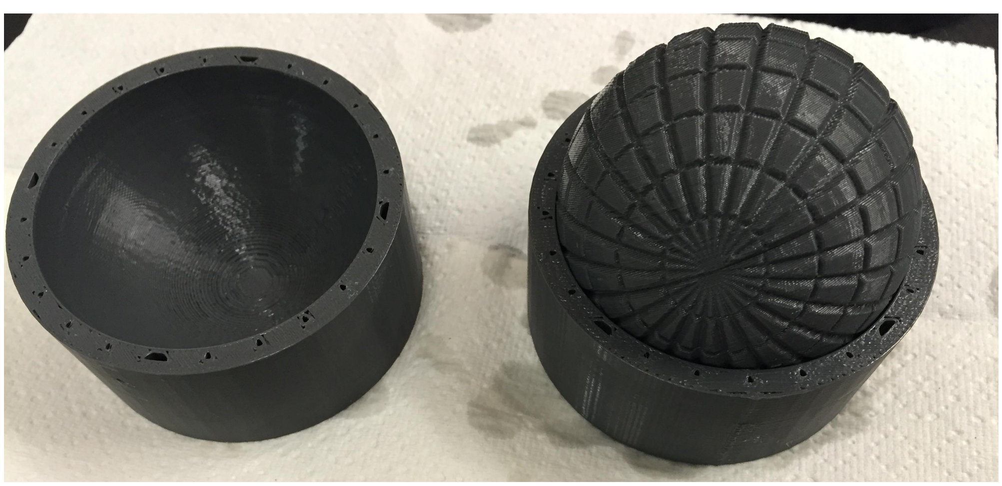

Figure 2: The dome phantom after it was 3D printed.

2.2 Image acquisition

Images of the star test pattern were acquired, by means of the dome phantom, using a Hologic DBT system (Hologic, Bedford, MA USA) in the Hospital of the University of Pennsylvania. One tomosynthesis image consists of 15 raw projections that are taken along a 15° arc. The star pattern was imaged at 45 mAs and 29 kVp with an aluminum filter and tungsten target. The detector of this system has 140 μm resolution, making the aliasing frequency 3.6 line pairs/millimeter (lp/mm).

The star pattern was imaged at four phantom angles of 0°, 45°, 90°, and 135°. These angles are all in the same plane of reconstruction. For each phantom angle, we imaged dome rotations at 0° and 90°. For each dome rotation, we imaged tilts from 0° to 180° in 15° increments. The dome phantom has the capability to image the star pattern in any orientation, so these results are only a sample of all the possible orientations.

Images of the star test pattern were obtained using the dome phantom on the breast support at the center of the detector's field of view and along the chest wall edge. We hypothesized that at the center of the detector, resolution would be symmetric about the tilt angle from 0° to 180° for some of the reconstructions. The dome phantom's encasement was secured to the breast support with paper and tape so that when the tilt angle was changed after every image, the phantom would not shift out of place.

2.3 Dome phantom rotations

The star test pattern was imaged in the dome phantom with a series of rotations (phantom, dome, and tilt). The phantom rotation refers to the rotation of the star test pattern within the dome hemispheres. Dome rotation is the rotation of the dome with respect to its cylindrical encasement about the z-axis; the dome orientation of 0° is represented in Figure 3. The source motion in Figure 3(a) is shown as linear for simplification, whereas the actual source motion is circular. The tilting of the star pattern is achieved with the y-axis acting as the axis of rotation in this example.

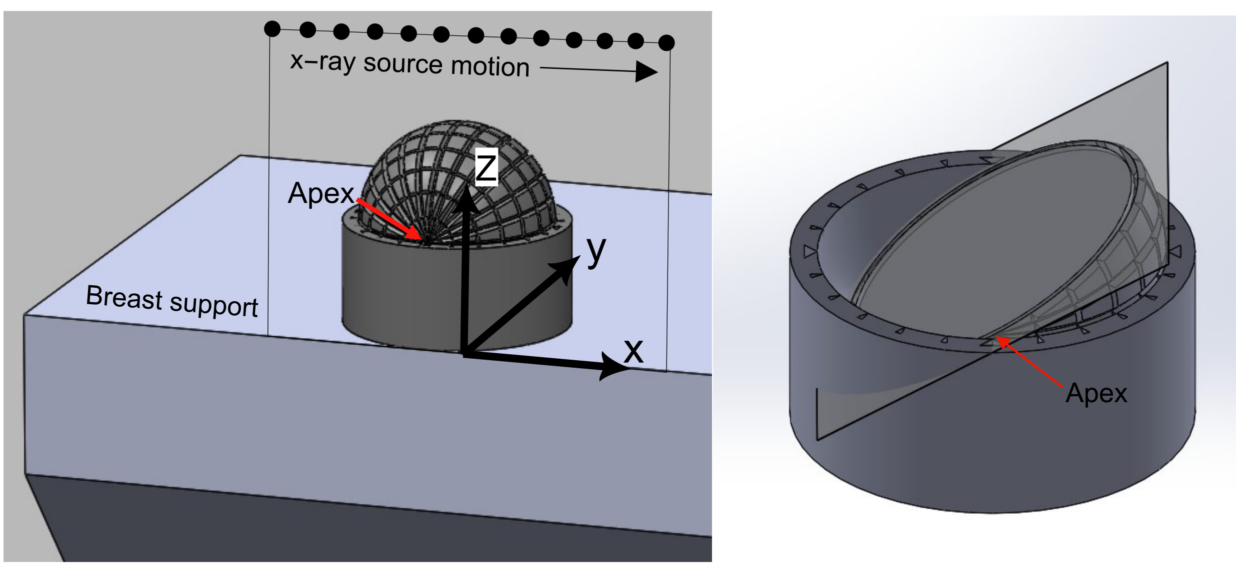

(a) (b)

Figure 3: This figure shows the illustration of the dome orientation of 0°. (a) Shows the plane of the x-ray source, the apex, and the coordinate system. (b) Is an example of an oblique tilt at the dome orientation of 0°.

For a dome rotation of 90°, the tilt rotations occur about the x-axis. In Figure 4, the dome is rotated about the z-axis by 90°. This changes the phantom orientations within the dome. Figure 4 illustrates this change for a dome rotation of 90°.

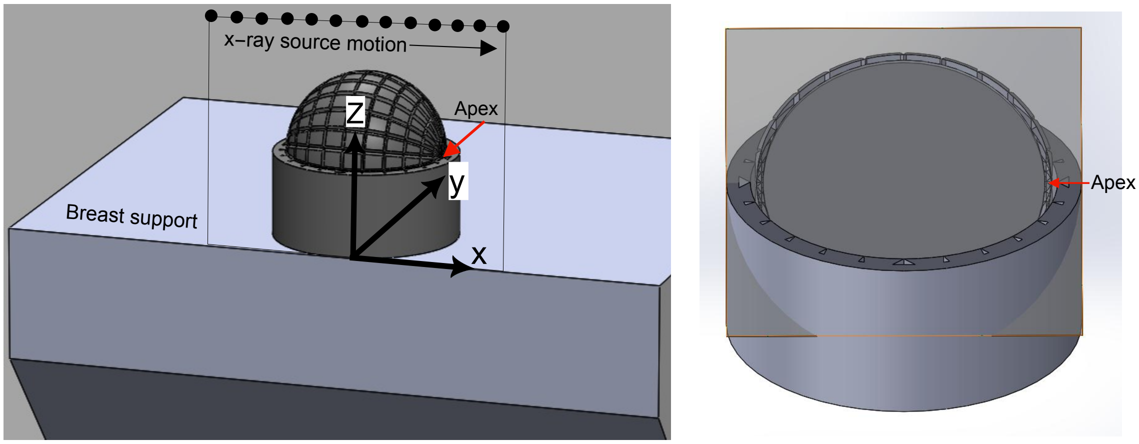

(a) (b)

Figure 4: This figure shows the illustration of the dome orientation of 90°. (a) Shows the plane of the x-ray source, the apex, and the coordinate system. (b) Is an example of an oblique tilt at the dome orientation of 90°.

The star test pattern has two sets of two perpendicular frequencies that are referred to as the phantom orientation. This allows for the analysis of two phantom orientations for each reconstruction plane, phantom orientations of 0° and 90° for example. The first set of frequencies analyzed were the phantom orientations of 0° and 90°, at the dome rotation of 0°. When the star pattern frequency is aligned with the positive x-axis, it refers to a phantom orientation of 0° at a 0° dome orientation.

2.4 Image reconstruction

The images were reconstructed using commercial reconstruction software, (Piccolo, Real Time Tomography, Villanova, PA). This software allows the reconstruction plane to match the plane of the star pattern. The reconstruction plane can be oriented to view the object at an orientation that is not parallel to the breast support. An illustration of a multiplanar reconstruction is displayed in Figure 5.

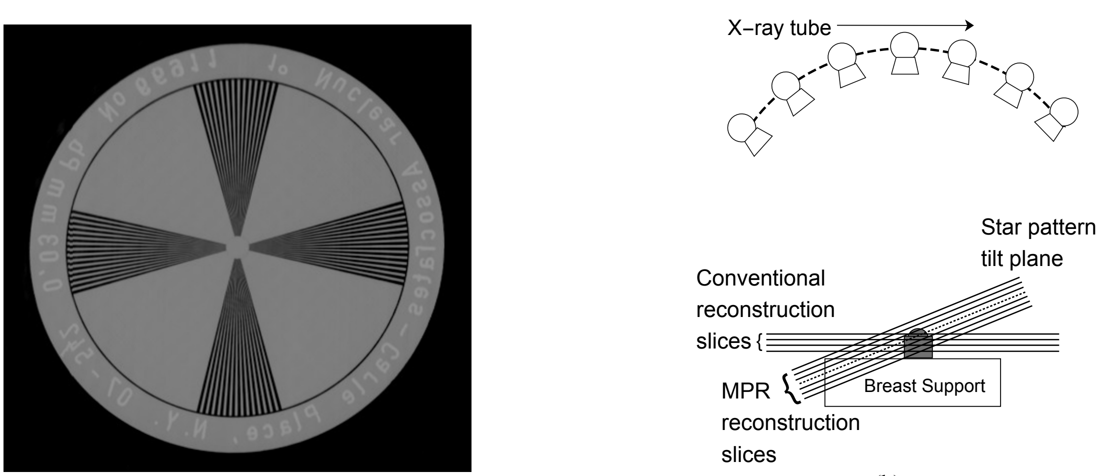

(a) (b)

Figure 5: This figure shows the orientation of the MPR reconstructions. (a) The plane view of the star pattern at a 30° tilt. (b) Is a diagram comparing the MPR reconstruction slices to the conventional slices.

2.5 Determinants of resolution

Once the images were reconstructed, two measures of spatial resolution were calculated. We quantified the resolution by calculating the limiting spatial frequency at the highest visible frequency. Contrast of the lowest spatial frequency (1.3 lp/mm) of the star pattern was also calculated. Once the images were reconstructed, we used the plot profile to perform the calculations.

2.6 Limiting spatial resolution and modulation contrast

Limiting spatial resolution was calculated by finding the maximum visible frequency of the star pattern in ImageJ[4]. This value was determined by finding the highest visible frequency for which there are 14 distinct wave peaks (and 15 wave troughs) in the plot profile. See Figure 6.

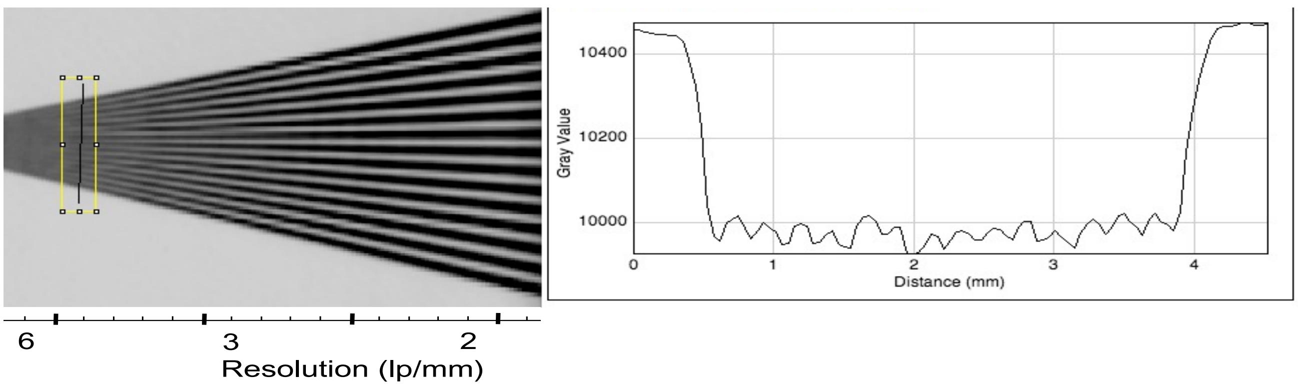

Figure 6: Example of the plot profile at the maximum visual spatial resolution.

The maximum visible frequency shows distinct wave peaks and troughs that are degraded in Figure 6. By inspection of the plot profile, one can see the 29 peaks and troughs. It is possible to calculate the maximum spatial resolution from this plot profile, but is easier at a lower frequency. Figure 7 is an example of more distinguishable peaks and troughs to show the principle of calculating the spatial resolution at a lower frequency with more certainty.

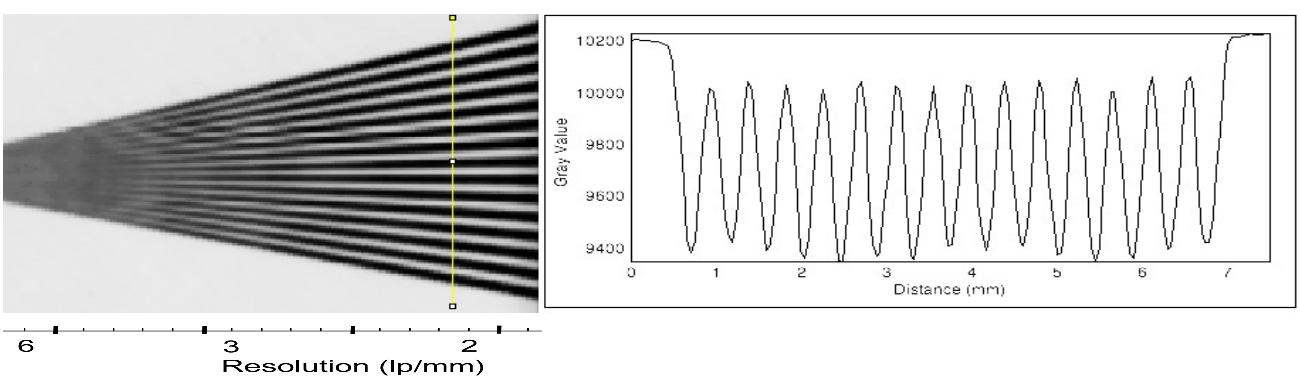

Figure 7: This is an example of the plot profile at a low frequency.

The calculation of limiting spatial resolution is represented in equation (1). For simplicity, the number of line pairs is represented by κ and the distance that the peaks span is represented by δ.

$$Resolution = \frac{line\ pairs}{distance\ (mm)} \equiv r = \frac{\kappa}{\delta} \quad (1)$$

The limiting spatial resolution was measured by visual inspection for each orientation ten different times ($n = 10$). This was done to perform the calculation of uncertainty in the limiting spatial resolution. The error represented in our results of the resolution is given by the standard 95% confidence interval in the following equation:

$$95\%\ confidence\ interval\ for\ r = \tilde{r} \pm 1.96\left(\frac{\sigma}{\sqrt{n}}\right) \qquad (2)$$

The σ in the equation represents the standard deviation and n represents the number of repetitions of the measurement. The yellow box in Figure 6 is an example of the visual representation of this error. This means that someone viewing this image would determine that the maximum visible frequency would be somewhere within this box. The value, $\tilde{r}$, is the average resolution of the ten measurements.

To calculate the contrast at every tilt, we measured the intensities at the lowest spatial frequency of the star-pattern in the plot profile. This is the point at which the frequencies meet the circumference of the circle around the star pattern. A representation of this analysis can be seen in Figure 8**.**

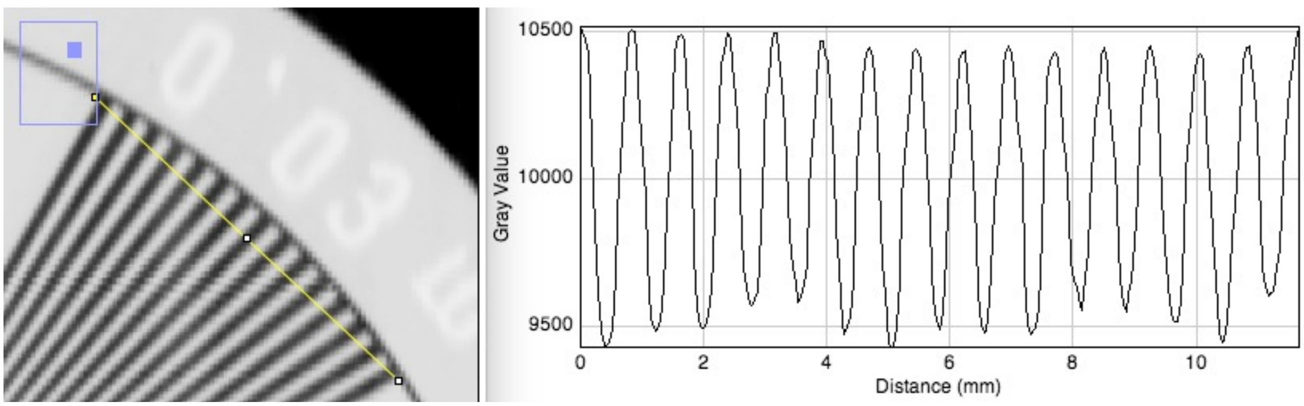

Figure 8: Modulation contrast is calculated where the frequency meets the circumference of the circle on the star pattern.

The modulation contrast is given by the Michelson equation:

$$Contrast \equiv C = \frac{I_{max} - I_{min}}{I_{max} + I_{min}} \qquad (3)$$

Contrast was calculated by determining the maximum and minimum gray values (I_{max}, I_{min}) in the plot profile for each line pair. As can be seen in the plot above, not all of the peaks and troughs are the same. Because of the deviation, the uncertainty was calculated by averaging the calculation of each line pair. The uncertainty is represented in the results by the 95% confidence interval, just like limiting spatial resolution. In this case, $n = 14$, (the number of whole line pairs) and $\tilde{C}$ is the average contrast for each line pair.

$$95\%\ confidence\ interval\ for\ C = \tilde{C} \pm 1.96\left(\frac{\sigma}{\sqrt{n}}\right) \qquad (4)$$

3. RESULTS

3.1 Dome orientation 0° and Phantom orientation 0°

This first orientation resembles the study conducted by Acciavatti in 2013[2]. At the 0° tilt, the frequency is parallel to the x-ray source motion. As the plane is tilted, super-resolution is expected based on previous work[2]. A diagram showing this orientation, along with the results of limiting spatial resolution and modulation contrast, can be seen in Figure 9**.**

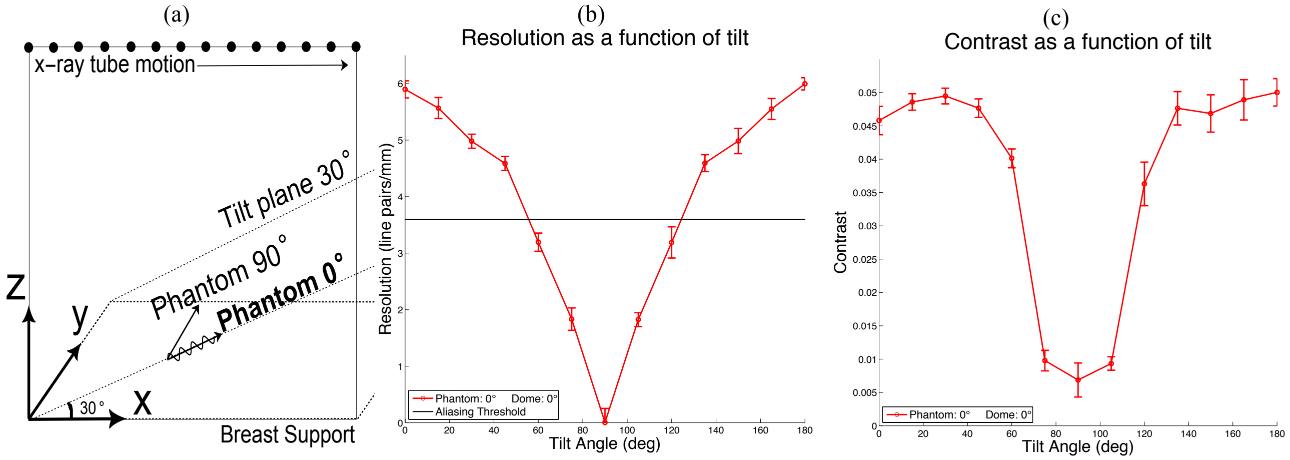

Figure 9: Diagram and results for the dome 0° and phantom 0° orientation.

In Figure 9(a), the frequency being analyzed is represented by the sinusoidal wave in the tilt plane. The black dots show the x-ray source positions for the scan. The diagram shows the tilt plane of 30° as an example. Figure 9(b) shows the calculated results for the limiting spatial resolution. The horizontal black line represents the alias frequency of the detector. Super-resolution is achieved up to a tilt angle of nearly 60°. Figure 9(c) shows the modulation contrast. Many of the confidence intervals overlap, suggesting that the modulation contrast is constant until higher tilt angles. The contrast does not degrade significantly until nearly 60°, like the graph of limiting spatial resolution. Figure 10 qualitatively shows the degradation of the limiting spatial resolution for this orientation.

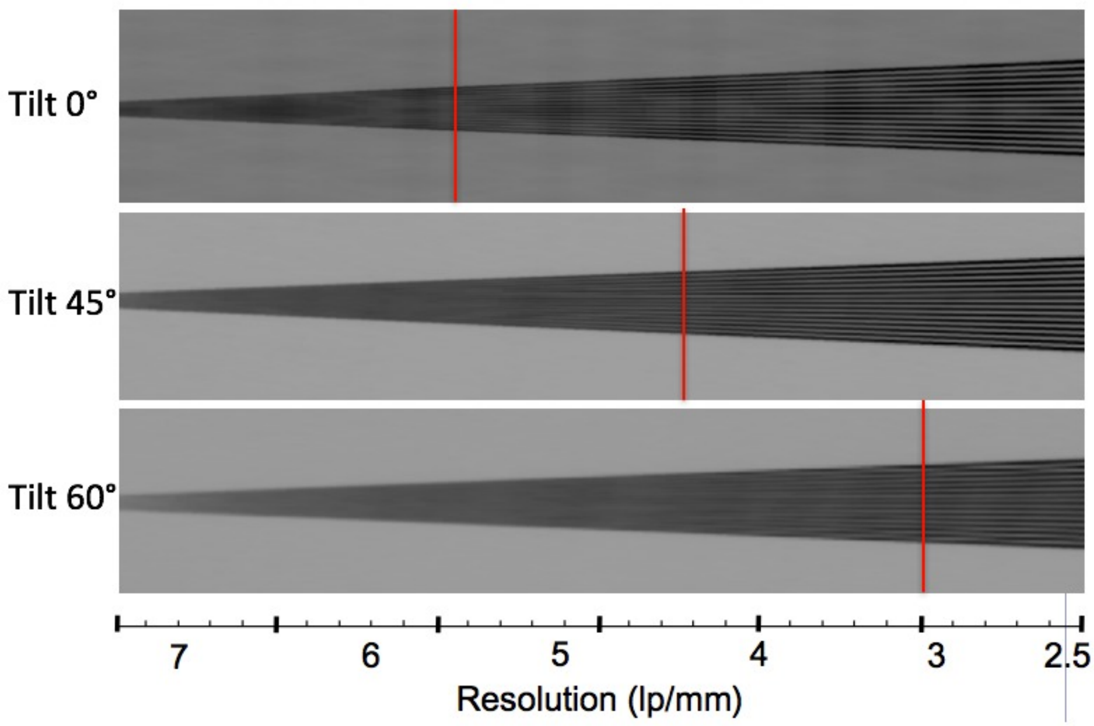

Figure 10: Limiting spatial resolution is shown in the images of the star pattern frequency for the phantom orientation of 0°

The highest limiting spatial resolution of the three sample angles in Figure 10 is seen at the 0° tilt. The limiting spatial resolution is near 6 lp/mm, coinciding with the results of Acciavatti[2,5]. The highest limiting spatial resolution at the 60° tilt is below the alias frequency of the detector.

The limit of resolution is higher in the reconstructions than it is in the raw projections. The raw projections also show more artifacts from the plastic of the dome phantom than the reconstructions. Figure 11 shows the difference between the central projection and the reconstruction. The limit of resolution in the reconstruction is near 6 lp/mm whereas the limit of resolution in the central projection is about 3 lp/mm.

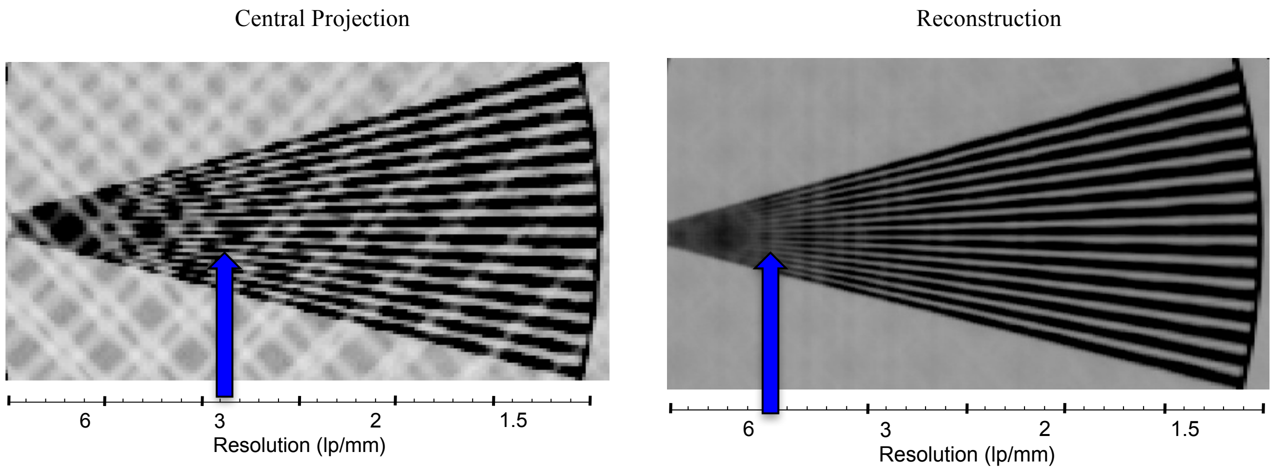

Figure 11: This figure shows the difference in quality between the central projection and the reconstruction.

3.2 Dome orientation 0° and Phantom orientation 90°

The second orientation analyzed is of the same reconstruction plane, but a different frequency. The phantom orientation of 90° corresponds to the frequency that is aligned perpendicular to the plane of x-ray source motion. The tilts of this orientation are the same as before. With the frequency perpendicular to x-ray source motion, it is assumed that aliasing will be present in the reconstructions and that there will be minimal change in resolution and contrast. The diagram and results of this orientation can be seen in Figure 12.

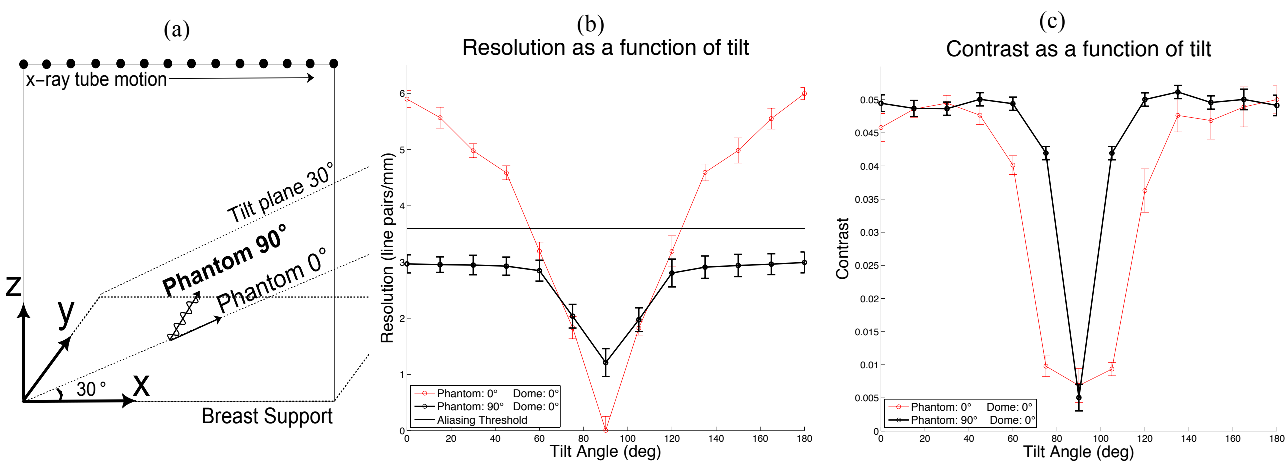

Figure 12: Diagram and results for the dome 0° and phantom 90° orientation.

The orientation being analyzed is again represented by the sinusoidal wave in the diagram. It is parallel to what is defined as the y-axis or the posteroanterior direction. The results of Figure 12(b) for limiting spatial resolution show that the resolution is constant up to a tilt angle of 60° and symmetric about the tilt angle of 90°. The resolution is always below the aliasing threshold, demonstrating that this orientation does not achieve super-resolution. For the modulation contrast, the error bars overlap to an even higher tilt angle than the phantom orientation of 0°.

3.3 Dome orientation 90° and Phantom orientation 0°

The dome rotation of 90° and the corresponding tilt angles are shown in Figure 13(a). This orientation also changes the plane of reconstruction. Now the tilt occurs about the x-axis. The 0° phantom orientation now corresponds to the frequency that is parallel to the y-axis at the 0° tilt. The diagram of this orientation and the results can be seen in Figure 13. The tilt now occurs about the x-axis, and as a result, there is more degradation of limiting spatial resolution as the obliquity increases. The limiting spatial resolution for this orientation is the lowest for all tilt angles. The current orientation shows degradation of limiting spatial resolution as low as 30° of obliquity. The modulation contrast shows the same pattern, degrading at lower tilt angles than the dome 0° and phantom 90° orientation, but the error bars still overlap at the lowest tilt angles.

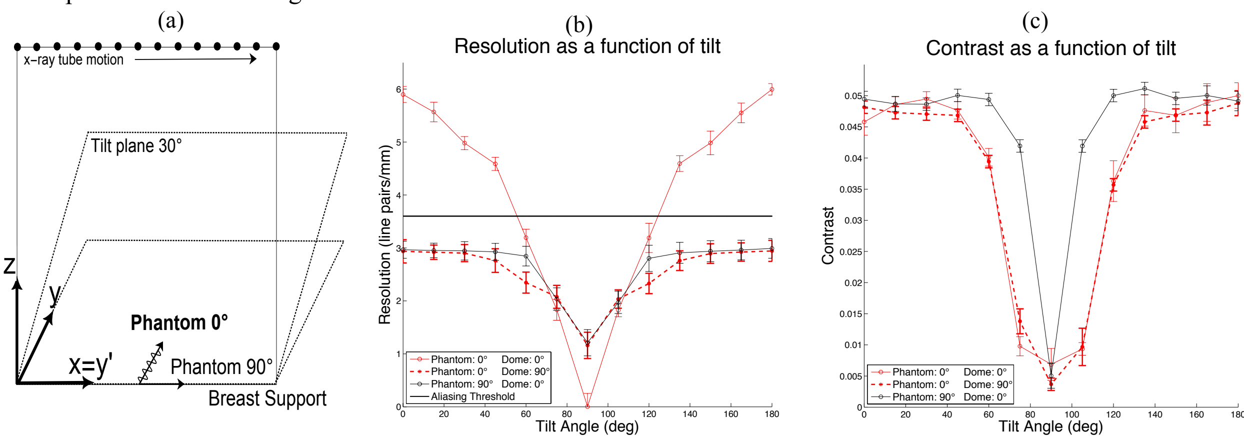

Figure 13: Diagram and results for the dome 90° and phantom 0° orientation.

3.4 Dome orientation 90° and Phantom orientation 90°

This orientation is the same reconstruction plane as section 3.3, but the frequency being analyzed is now different. The frequency is parallel to the x-ray source motion at all tilt angles. There is minimal change in the limiting spatial resolution and contrast until higher obliquities. The diagram and results for this orientation can be seen in Figure 14. This orientation shows the broadest range of angles that achieve super-resolution. Most of the reconstruction planes have a limiting spatial resolution value around 6 lp/mm. The only angle for which super-resolution is not achieved is the 90° tilt orientation. The modulation contrast also remains high and constant for the same number of tilt angles as the dome 0° and phantom 90° orientation.

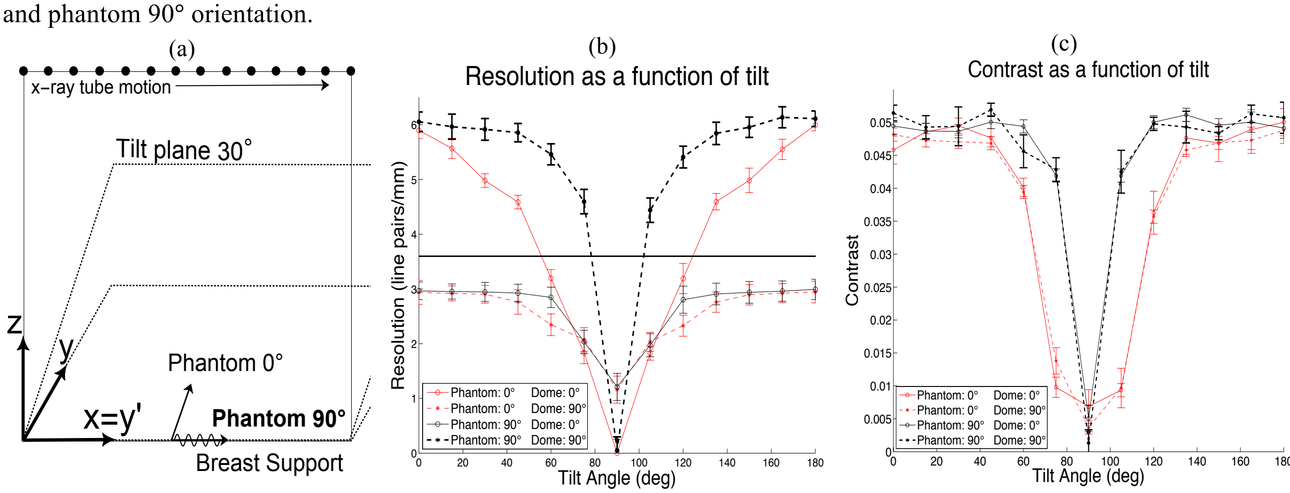

Figure 14: Diagram and results for the dome 90° and phantom 90° orientation.

3.5 Dome orientation 0° and Phantom orientations 45° and 135°

The following two orientations correspond to a phantom rotation within the dome. The phantom orientation of 45° reorients the frequencies that are being analyzed. This phantom rotation now aligns the frequency across the diagonal of the pixels in the detector. This changes the aliasing frequency to 5.09 lp/mm, which is given by: $3.6\ (\mathrm{lp}/mm) \cdot \sec(45°)$. This phantom rotation is shown in Figure 15. The tilts are the same as they were for the dome orientation of 0° in Figure 3. The results of this orientation for both of the phantom angles of 45° and 135° can be seen in Figure 16.

Phantom orientations 0° and 90°

Phantom orientations 45° and 135°

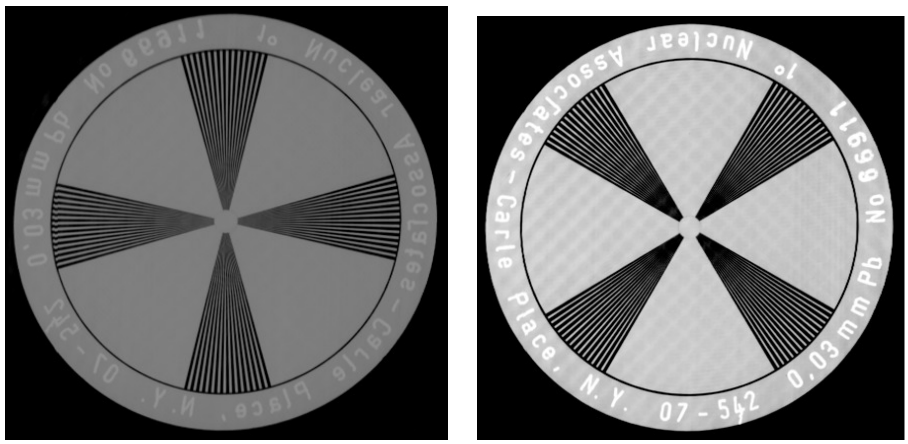

Figure 15: Example of the change in orientation for a phantom rotation of 45°.

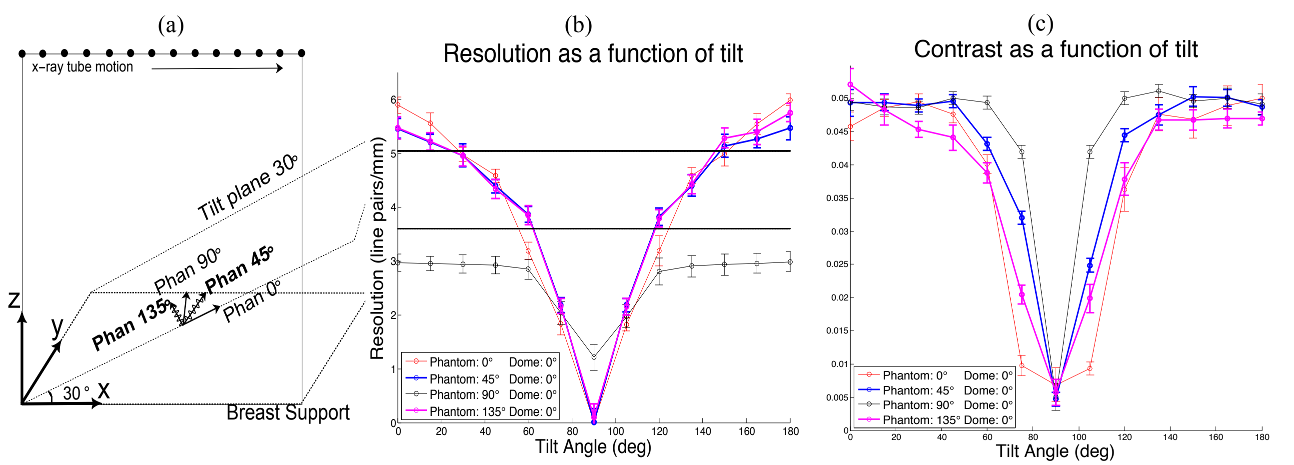

Figure 16: Diagram and results for the dome 0° and phantom 45° and 135° orientations.

These two orientations are shown together because of their symmetry. The results shown are very similar. For limiting spatial resolution (b), all of the confidence intervals for the 45° overlap with those of the 135° orientation. It is important to note that the aliasing frequency required to achieve super-resolution has now changed to the thicker black horizontal line at 5.09 lp/mm. This means that for these two phantom orientations, super-resolution is only achieved until an obliquity of just under 30°.

3.6 Dome orientation 90° and Phantom orientations 45° and 135°

The final orientation that was analyzed was of a dome rotation of 90° for the previous phantom orientations. This changes the orientation of the tilts to be about the x-axis. The orientation of the frequencies that are being analyzed has now changed. The aliasing frequency for this orientation is still 5.09 lp/mm. The diagram and results of this orientation can be seen in Figure 17.

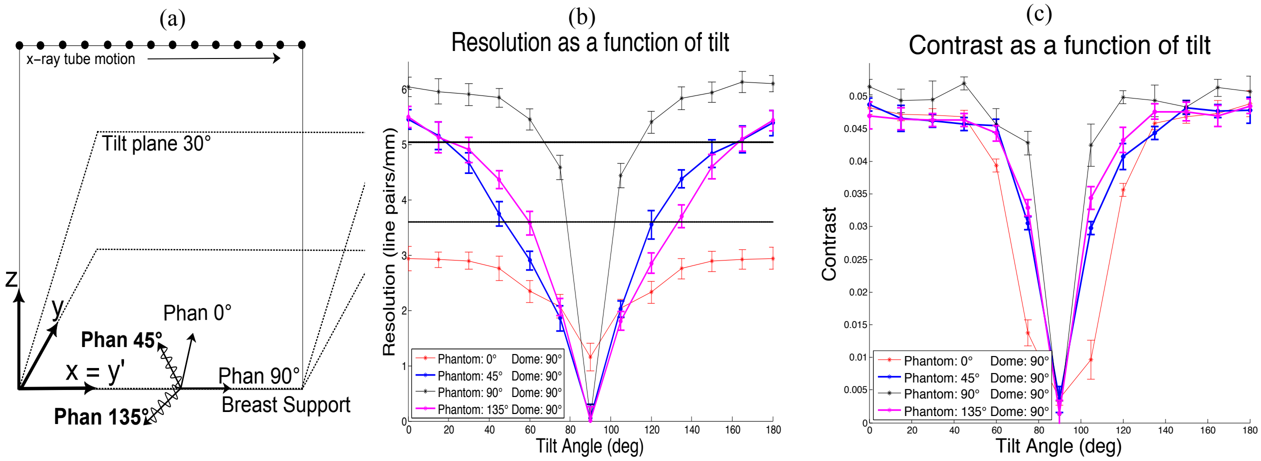

Figure 17: Diagram and results for the dome 90° and phantom 45° and 135° orientations.

These results show the lowest range of obliquities that achieve super-resolution. It is important to note, however, that the phantom orientations of 45° and 135° are anti-symmetric about the tilt angle of 90°. The phantom orientation of 135° has higher limiting spatial resolution than the orientation of 45° until an obliquity of 90° and vice-versa from 90° to 180°. While we need to do further experiments, one possible explanation for the anti-symmetry is that the limiting resolution is determined in part by the geometric magnification.

4. DISCUSSION AND CONCLUSION

We have shown that tomosynthesis supports oblique reconstructions over a broad range of obliquities. We have quantified the quality of oblique reconstructions in terms of low-frequency contrast and limiting spatial resolution. Low-frequency contrast is nearly constant over a broad range of obliquities. The contrast does drop to near zero at high obliquities. We have also shown that limiting spatial resolution decreases with increasing obliquity. Super-resolution is achieved for any component of the frequencies that are aligned parallel to x-ray source motion. This was previously shown by Acciavatti[2] in 2013. That study was conducted at the dome 0° and phantom 0° orientation. We verified that super-resolution is not achieved for frequencies perpendicular to x-ray source motion. We verified that super-resolution and the alias frequency vary with phantom angle due to the orientation of the frequency with respect to the detector's pixels.

The dome MPR phantom is a useful tool in analyzing limiting spatial resolution, but had limitations. Due to its construction, the dome phantom interfered with the calculation of modulation contrast. The plastic filament created artifacts in the images for orientations at low obliquities, and few artifacts for the higher obliquities. Inside of the dome phantom, the density of the plastic filament differs, and the x-ray images show a cross pattern. The pattern of artifacts resulted in high uncertainties for the calculation of modulation contrast at lower obliquities. They did not interfere with the calculation of limiting spatial resolution. Figure 18 shows more prominent artifacts at the plane of 0° tilt and less prominent artifacts at the plane of 30° tilt. Future MPR phantoms will be printed using solid materials.

The dome MPR phantom is capable of orienting the star pattern in any plane. This study considered only two dome rotations, but many other dome rotations should be analyzed with the corresponding tilts. Additional phantom angles within the dome should also be analyzed. A total of 104 frequency orientations have been analyzed with this data set. The dome phantom is capable of orienting the star pattern at 15° incremental angles for dome rotations, tilt rotations, and phantom rotations from 0° to 360°. Future MPR phantoms will support finer angular increments.

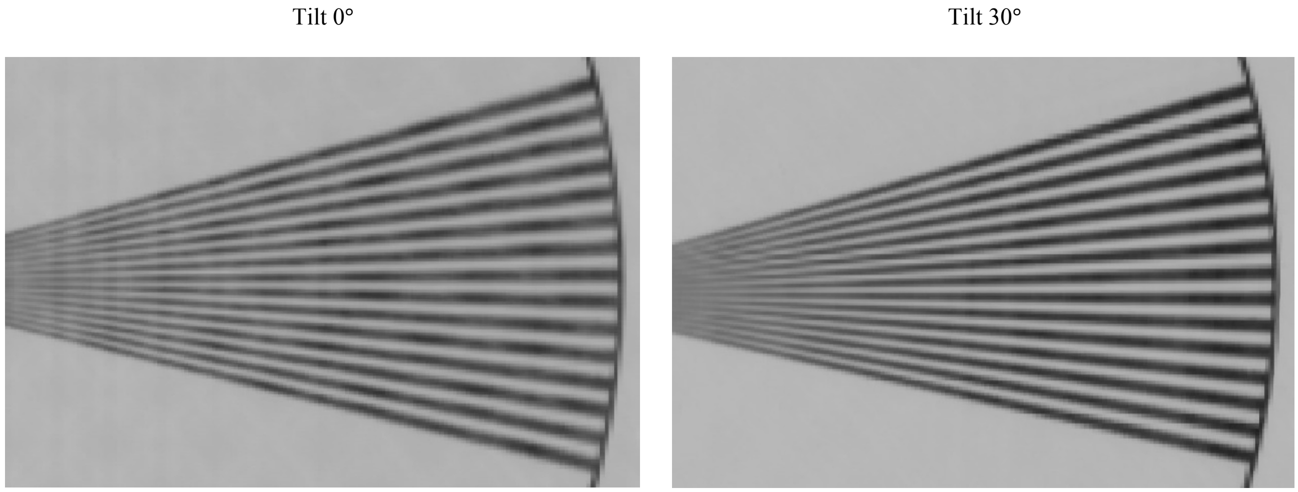

Figure 18: The artifacts at a 0° tilt are more prominent than at a 30° tilt for a dome rotation of 0°.

Concerning calculations of limiting spatial resolution and modulation contrast, the error is assumed to have a Gaussian distribution. Thus the variables of C and r of equations 1 and 3 assume Gaussian distribution. An analysis of this representative error will be investigated in the future. As the results suggest, the dependence of resolution and contrast with respect to the position of the dome phantom on the breast support should also be analyzed for MPR. We assume that the plots as a function of tilt angle will not necessarily be symmetric about 90° for different positions of the dome phantom on the breast support. This concept will be investigated in future work.

ACKNOWLEDGEMENTS

This work was supported by grants from the Susan G. Komen Foundation (PDF14302589 and IIR13264610) and NIH/NCI grant 1R01CA154444. TLV was supported by a Summer Undergraduate Research Fellowship from the American Association of Physicists in Medicine. ADAM receives research support from Hologic, Inc. The content is solely the responsibility of the authors and does not necessarily represent the official views of the funding agency.

The authors thank Johnny Kuo, Susan Ng, and Peter Ringer (Real Time Tomography, LLC, Villanova, PA) for technical assistance. ADAM is a shareholder of Real Time Tomography, and serves as a member of the scientific advisory board. The 3D printing was provided *gratis* from the University of Pennsylvania Biomedical Library.

REFERENCES

[1] Bartlett, E. et al. American Journal of Neuroradiology, vol. 27, pp. 13-19. (2006).

[2] R. Acciavati and A. D. A. Maidment, "Oblique reconstructions in tomosynthesis. II. Super-resolution," Medical Physics, vol. 40, no 11, pp. 111912-1 to 111912-19 (2013).

[3] R. J. Acciavatti and A. D. A. Maidment, "Oblique reconstructions in tomosynthesis. I. Linear systems theory," Medical Physics, vol. 40, no. 11, pp. 111911-1 to 111911-21 (2013).

[4] Rasband, W.S., ImageJ, U. S. National Institutes of Health, Bethesda, Maryland, USA, http://imagej.nih.gov/ij/, (1997-2015).

[5] R. Acciavatti and A. Maidment, "Observation of super-resolution in digital breast tomosynthesis," Medical Physics, vol. 39, no. 12, pp. 7518-7539, (2012).